Korean J. Chem. Eng., **28**(8), 1779-1784 (2011)
DOI: 10.1007/s11814-011-0002-z

Thermomechanical properties of ethylene-propylene-diene terpolymer/organoclay nanocomposites and foam processing in supercritical carbon dioxide

Young-Wook Chang†, Sunkeun Kim, Shin Choon Kang, and Seong-Youl Bae

Department of Chemical Engineering, Hanyang University, Ansan 425-791, Korea
(*Received 27 September 2010 • accepted 3 January 2011*)

Abstract−EPDM/organoclay nanocomposites were prepared by a melt mixing of a semicrystalline EPDM grafted with maleic anhydride and an organoclay (Cloisite 20A) in an internal mixer. XRD and TEM analysis revealed that the EPDM/clay forms a partially exfoliated nanocomposite and the silicate layers of the clay are uniformly dispersed at a nanometer scale in the rubber matrix. DSC studies indicated that the clay nanoparticles caused an increase in the nonisothermal crystallization temperature of the EPDM. Tensile and dynamic mechanical analysis showed that a small amount of the clay nanoparticles effectively enhanced the stiffness of the EPDM without adversely affecting its flexibility. The EPDM/clay nanocomposites were used to produce foams by using a batch process in an autoclave, with supercritical carbon dioxide as a foaming agent. The exfoliated nanocomposite produced a microcellular foam with average cell size as small as 6.23 μm and cell density as high as 2.4×10^{10} cell/cm^3.

Key words: EPDM, Organoclay, Nanocomposite, Thermomechanical Properties, Microcellular Foam, Supercritical Carbon Dioxide

INTRODUCTION

Polymer nanocomposites containing plate-like clay nanoparticles have gained attention in recent decades because of their superior properties when compared with their microcomposite counterparts. Montmorillonite, a 2 : 1 layered smectite clay, is the most often used clay, containing several thousand individual layers having thickness of 1 nm and lengths on the order of 100-1,000 nm stacked together. Exfoliation and homogeneous dispersion of these layers in polymer matrix is possible when the clay surface is organically modified via an exchange metal cation located between the individual layers by a long-alkyl ammonium ion. The organically modified clay becomes hydrophobic and gallery height of the clay is expanded, which facilitates the intercalation of polymer molecules between the layers of the clay [1-3]. Melt compounding using conventional high shear mixers offers an efficient way to fabricate the polymer nanocomposites, which is especially effective for polar thermoplastics such as nylons [4,5], polyesters [6,7], polyetherimide [8], and so on.

In the case of non-polar polyolefins like polystyrene, polyethylene and polypropylene the nanocomposites can be obtained only when a polar compatibilizer is added or the matrix polymer is modified with a polar functional group such as oxazoline or maleic anhydride [9-11]. Wang et al. [12], in their studies on maleated polyethylene/organoclay nanocomposites by a melt mixing found that if the number of methylene units in alkylammonium chain of organoclay is larger than 16, delamination of the organoclay could be obtained when the grafting level of maleic anhydride on the polymer backbone exceeds 0.1 wt%. These nanocomposites, with only a small percentage of clay, exhibit greatly enhanced properties such as high strength, high modulus, high thermal stability and increased barrier property relative to the virgin polymers.

Microcellular low-density polymeric foams, characterized by cell sizes smaller than 10 μm and cell densities larger than 10^9 cells/cm^3, are of interest because they have high stiffness-to-weight ratios and excellent mechanical properties compared with common structural foams at equivalent densities [13,14]. Recently, it was found that microcellular foams could be fabricated with polymer/clay nanocomposites using supercritical carbon dioxide as a blowing agent, which include polypropylene/clay [15,16], polycarbonate/clay [17, 18], polylactide/clay [19,20], polystyrene/clay [21,22], polymethylmethacrylate/clay [23], and polyethylene-octene/clay [24] nanocomposites. These studies revealed that incorporation of clay nanoparticles reduced the cell sizes and increased the cell density of the foams as compared to the foam obtained with pure polymer, and the cellular structure is dependent upon the clay dispersion as well as type of polymers and foam processing conditions.

Ethylene-propylene-diene terpolymer (EPDM) is an important elastomer widely used in applications such as foamed sheet, automotive parts, durable goods and wire and cable owing to its outstanding heat, ozone and weather resistance and excellent electrical insulating properties. EPDM with high ethylene content (higher than 70%) has a certain degree of crystallinity and the crystalline domains form physical crosslinking. The semicrystalline EPDM behaves like a thermoplastic elastomer exhibiting high elastic recovery as well as melt processability. To our knowledge, studies on the semicrystalline EPDM/clay nanocomposites and their microcellular foams have not been reported so far. In this study, we prepared an exfoliated/intercalated nanocomposite from the semicrystalline EPDM grafted with a small amount of maleic anhydride and an organoclay via melt blending method. Thermomechanical properties of the nanocomposite and the possibility of fabrication of microcellular foam with the nanocomposite using supercritical carbon dioxide as a blow-

†To whom correspondence should be addressed.
E-mail: ywchang@hanyang.ac.kr

ing agent was evaluated.

EXPERIMENTAL

1. Materials

Semicrystalline EPDM grafted with 0.5% maleic anhydride content (Royaltuf 485) was purchased from Crompton Co. (Seoul, Korea). The clay mineral used in this study is a Cloisite 20A (Southern Clay Products), which is a natural Na^+ montmorillonite modified with a quaternary ammonium salt, dimethyl dihydrogenated tallow ammonium chloride,

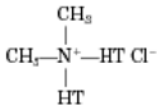

where HT is a hydrogenated tallow which consisted of *ca* 65% C18, 30% C16 and 5% C14 units.

2. Preparation of EPDM/Clay Nanocomposite

All materials were dried under vacuum (30 in Hg) at 50 °C for 5 hr before use. The composites were prepared by melt blending in an internal mixer (Haake Polylab 600) using a rotor speed of 60 rpm and at a temperature of 150 °C for 10 min. The amount of organoclay was 5, 7 and 10 parts per hundred rubber (phr). The obtained compounds were compression molded into test pieces.

3. Foam Processing

The polymer sample of 1 mm thick was first placed in an autoclave connected to a carbon dioxide cylinder. The samples were then saturated with carbon dioxide at a predetermined foaming temperature (125, 130 and 135 °C) and pressure (30 MPa). After the complete solubilization of the gas in the polymer melt was reached, the CO_2 pressure was reduced rapidly to atmospheric conditions. The system was maintained at zero pressure for approximately 1 hour so that the bubbles could grow completely.

4. Characterizations

Change of gallery distance in the clay after mixing it with the rubber was examined using X-ray diffraction patterns recorded on a diffractometer (BEDE D-3 system) using CuKα radiation (λ= 1.54 Å) at a generator voltage of 40 kV and a generator current of 100 mA. Dispersibility of the silicate layers in the composite was evaluated using transmission electron microscopy (TEM). TEM micrographs were obtained with a JEOL 200CX TEM using an acceleration voltage of 200 kV.

Non-isothermal crystallization and melting temperatures of pure polymer and its hybrids were determined with a differential scanning calorimeter (TA Instrument DSC 2010). 10 mg of the samples dried completely in vacuum oven was used for the analysis. It was heated from 30 °C to 160 °C at a rate of 10 °C/min under a nitrogen atmosphere and was kept for 10 min at this temperature to remove thermal history. Then the sample was cooled to 30 °C at a rate of −10 °C/min to induce non-isothermal crystallization. The non-isothermally melt crystallized sample was heated again to 160 °C at a rate of 10 °C/min to observe melting behavior.

The ultimate tensile strength, elongation at break, and tensile moduli were determined with a universal testing machine (United Co., STM-10E) at 25 °C and with a crosshead speed of 500 mm/min, according to ASTM D412 specifications.

Dynamic mechanical properties of the composites were determined by a dynamic mechanical analyzer (TA instrument DMA 2980). The sample was subjected to a cyclic tensile strain with an amplitude of 0.2% and a frequency of 10 Hz. The temperature was increased at a heating rate of 2 °C/min from −100 to 200 °C.

For the observation of cell structure of the foamed samples, they were fractured using liquid nitrogen and sputter coated with gold and were examined by scanning electron microscopy (SEM, Jeol 1100). The mass density of both pre-foamed ρ_p and post-foamed ρ_f in g/mL samples was estimated by using the method of buoyancy. The average cell size d in μm was determined from the data of SEM observation. The cell densities N_c in cell/cm^3 and mean cell wall thickness δ in μm were determined by using the following equations [20,23]:

$$N_c=10^4[1-(\rho_f/\rho_p)]/d^3 \quad (1)$$

$$\delta=d\,[1/(1-(\rho_f/\rho_p))^{0.5}-1] \quad (2)$$

RESULTS AND DISCUSSION

1. Structure of EPDM/Clay Hybrids

Fig. 1 shows the XRD patterns of organoclay and the EPDM/clay with different clay loadings. The peak corresponding to the basal spacing of the organoclay (Cloisite 20A) appears at 2θ=3.55° (the corresponding d_{001} spacing is 2.5 nm). It can be clearly seen that the diffraction peak for the EPDM/clay systems appears at a much lower angle relative to that for the organoclay, indicating that polymer chains are intercalated into the layers of the organoclay. It can also be seen in the figure that the diffraction peak in EPDM/clay becomes shallow and broad as compared to that of the organoclay, which is associated with a decrease in the coherent layer scattering. The intercalation of polymer chains inside the clay particles disorders the layered structure of the clay and, thus, a decrease in the XRD coherent layered scattering is observed [25,26]. Agglomerates of clay particles are also observed in the nanocomposite containing 10 phr clay. This partially exfoliated structure was generally observed in the majority of the polymer-clay nanocomposites.

The degree of dispersion of the clay nanoparticles can be directly

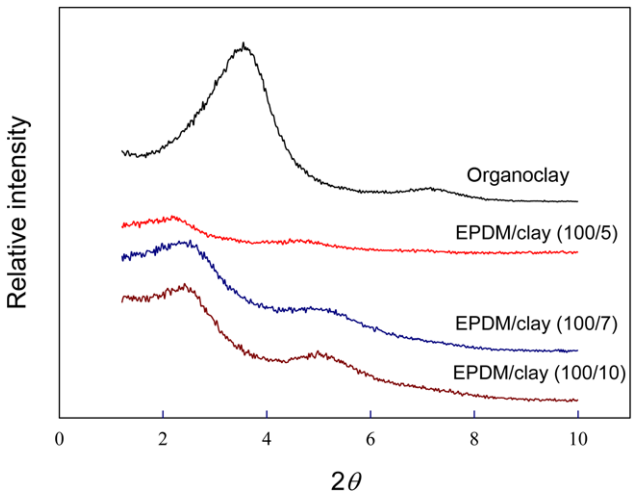

Fig. 1. X-ray patterns of organoclay and EPDM/clay nanocomposites with different clay loadings.

(a)

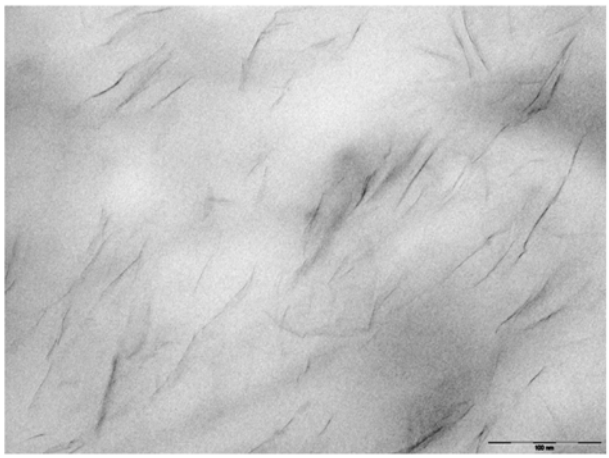

(b)

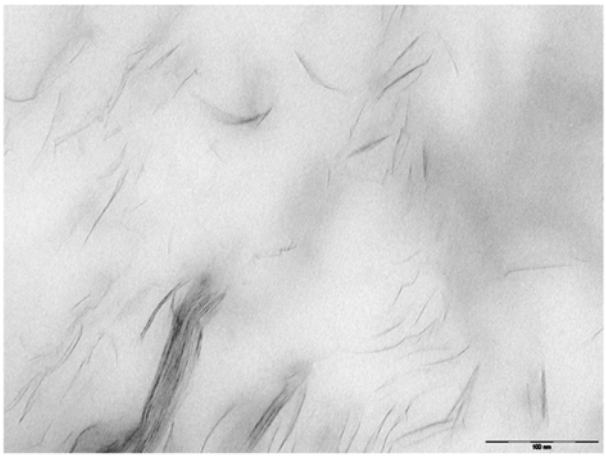

(c)

Fig. 2. TEM image of EPDM/clay nanocomposites with different clay loadings (a) 5 phr (b) 7 phr (c) 10 phr.

seen in TEM photographs of ultrathin section of a compression-molded EPDM/clay with clay loading of 5, 7 and 10 phr, which are shown in Fig. 2. The dark lines are the cross sections of the clay layers and it can be seen that the clay particles of 10-30 nm thickness were dispersed uniformly in the polymer matrix when the clay content is 5 phr. Also, the clay particles tend to agglomerate with increasing clay content.

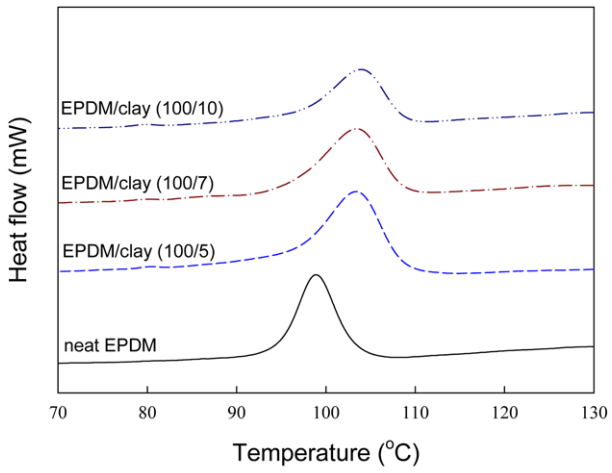

(a)

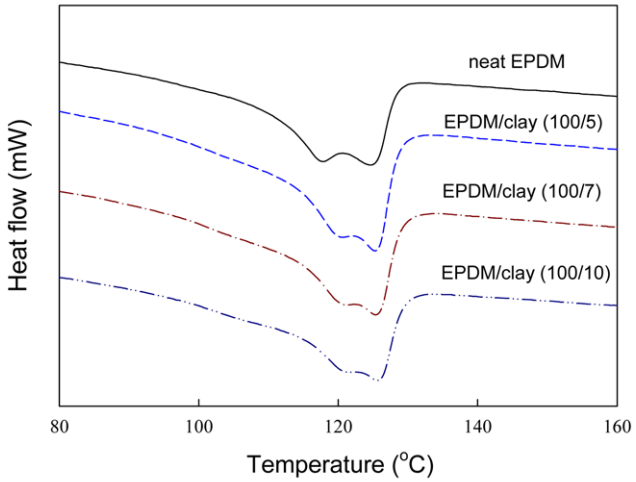

(b)

Fig. 3. (a) Crystallization exotherms (b) melting endotherms of EPDM and EPDM/clay nanocomposites with different clay loadings.

Table 1. DSC data of EPDM/clay nanocomposites

Clay contents (phr)	T_c (°C)	ΔH_c (J/g)	T_{m1} (°C)	T_{m2} (°C)
0	98.9	10.1	118.0	124.8
5	103.4	10.0	119.6	125.3
7	103.5	10.8	120.2	125.5
10	104.0	10.5	121.8	125.6

2. Thermal Properties

The EPDM employed in this study is a semi-crystalline material, so the crystallization and melting behavior of the polymer might be affected by the clay nanoparticles. DSC thermograms of non-isothermal crystallization and re-melting process for pure EPDM and EPDM/clay nanocomposites are shown in Fig. 3(a) and (b), respectively, and the results are summarized in Table 1. In the cooling process of DSC measurement, the nanocomposites show higher crystallization peak temperatures (T_c) than neat EPDM. The T_c is increased by 4.5 °C on the addition of 5 phr clay, and it increased

slightly with further addition of the clay. The increase in T_c indicates an increased crystallization rate in the nanocomposites. Increase in the crystallization rate has been widely observed in semicrystalline polymer/clay nanocomposites, in which clay nanolayers can adsorb polymer chains more easily and the clay particles act as nucleating agents [7,9,13]. In the remelting processes, shown in Fig. 3(b), pure EPDM and its nanocomposites showed double melting behavior, indicating that two different types of crystalline structure exist in the polymer. There is slight increase in the two melting temperatures in the presence of clay.

3. Mechanical Properties

Reinforcement effect of clay nanoparticles in the EPDM/clay nanocomposites was examined by tensile and dynamic mechanical measurement. The results of tensile testing, including the modulus at a given strain, tensile strength and elongation at break, are shown in Table 2. It is observed from the table that tensile modulus and

Table 2. Tensile properties of pure EPDM and EPDM/clay nanocomposites

Clay contents (phr)	Modulus at a given extension (MPa)			Tensile strength (MPa)	Elongation-at-break (%)
	50%	100%	300%		
0	1.08	1.35	1.66	1.91	649
5	1.67	2.00	2.32	2.23	720
7	1.95	2.34	2.77	2.64	607
10	1.99	2.35	2.80	2.73	550

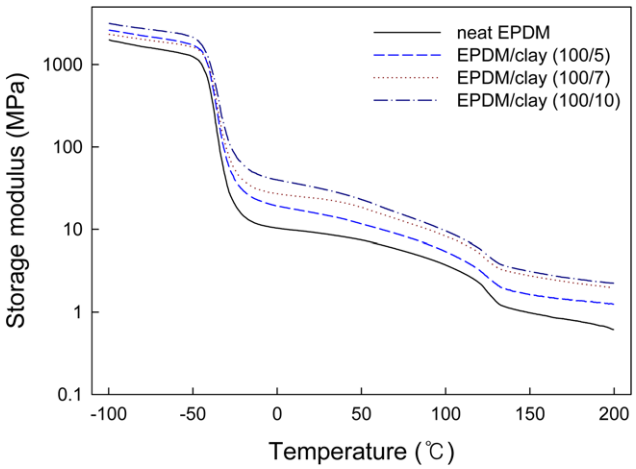

Fig. 4. Temperature dependence of dynamic storage moduli of pure EPDM and EPDM/clay nanocomposites with different clay loadings.

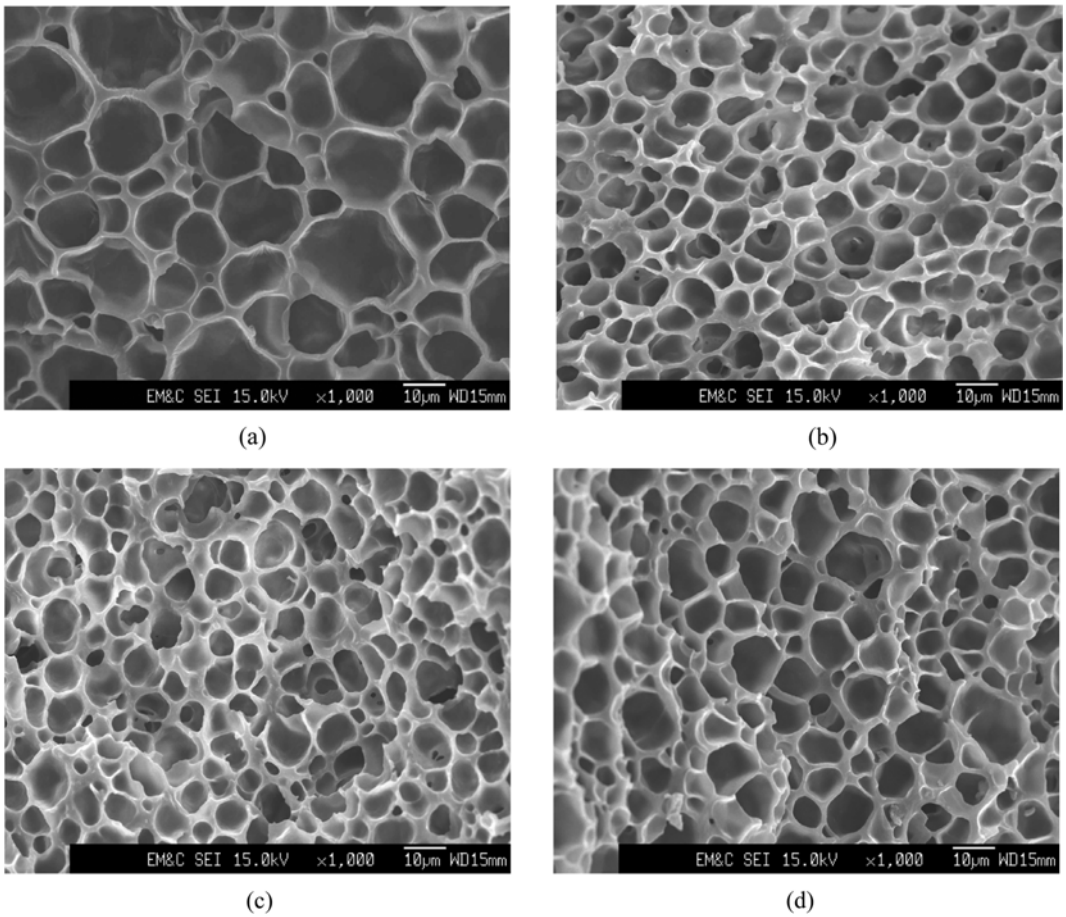

Fig. 5. SEM images of the freeze-fracture surface of foams from pure EPDM and EPDM/clay nanocomposites with different clay loadings (foaming temperature: 130 °C).

strength increased with increasing clay content. For example, 100% and 300% modulus of the EPDM/clay (100/5) is 1.48 times and 1.39 times higher than those of the pure EPDM, respectively. It is noted from the table that the increase in the modulus in the nanocomposites is accompanied by retention of ductility of pure EPDM. Similar trends in the tensile behavior were also observed in other rubber/clay nanocomposites such as polyurethane elastomer/clay nanocomposites [27,28]. This is in contrast to the tensile behavior of conventional elastomer composites containing micron-sized inorganic fillers, in which the elastic modulus is typically enhanced with sacrificing the elongation at break [29].

Reinforcing effect of the clay nanoparticles could also be seen from the temperature dependence of dynamic storage moduli (E′) of the samples, which are presented in Fig. 4. It is obvious that EPDM/clay nanocomposites exhibited higher storage modulus than pure EPDM over the entire temperature range. For example, E′ at 40 °C and 120 °C of the EPDM/clay (100/5) is 2.0 times and 2.2 times higher than that of the pure EPDM. Such an effective modulus enhancement on the addition of small amount of clay particles in the nanocomposite is attributed to the huge interfacial action between the polymer and clay nanoparticles.

4. Foam Processing and Cellular Structure

Fig. 5 shows the results of SEM images of the freeze-fracture surfaces of the neat mEPDM foam and mEPDM/clay nanocomposites foams, which were foamed at 130 °C. All foams exhibit a closed-cell structure. From SEM images, various morphological parameters of the foams were calculated and these are summarized in Table 3. It is noted that pure EPDM foam has an average cell size of 12.0 μm and the cell density of 4.2×10^{9} cell/cm^3. For EPDM/clay (100/5) nanocomposite foam, cell size is reduced to 6.2 μm, and the cell density increases to 2.4×10^{10} cell/cm^3, about 5.7 times larger than that of the pure EPDM foam. But, with higher clay content, the cell size is slightly increased and the cell density is decreased. And the cell wall thickness decreased from 2.06 μm for pure EPDM foam to 1.93 μm for EPDM/clay (100/5) nanocomposite foam. In the heterogeneous nucleation system containing filler particles, cell nucleation takes place in the boundary between the matrix polymer and the dispersed filler particles. The increase in the cell density in

Table 3. Morphological parameters of neat EPDM foam and EPDM/clay nanocomposite foams

Clay contents (phr)	ρ_f (g/cm^3)	d (μm)	N_c (cell/cm^3)	δ (μm)
0	0.23	12.0	4.21×10^{9}	2.06
5	0.37	6.23	2.40×10^{10}	1.93
7	0.35	7.47	1.47×10^{10}	2.08
10	0.27	8.55	1.12×10^{10}	1.63

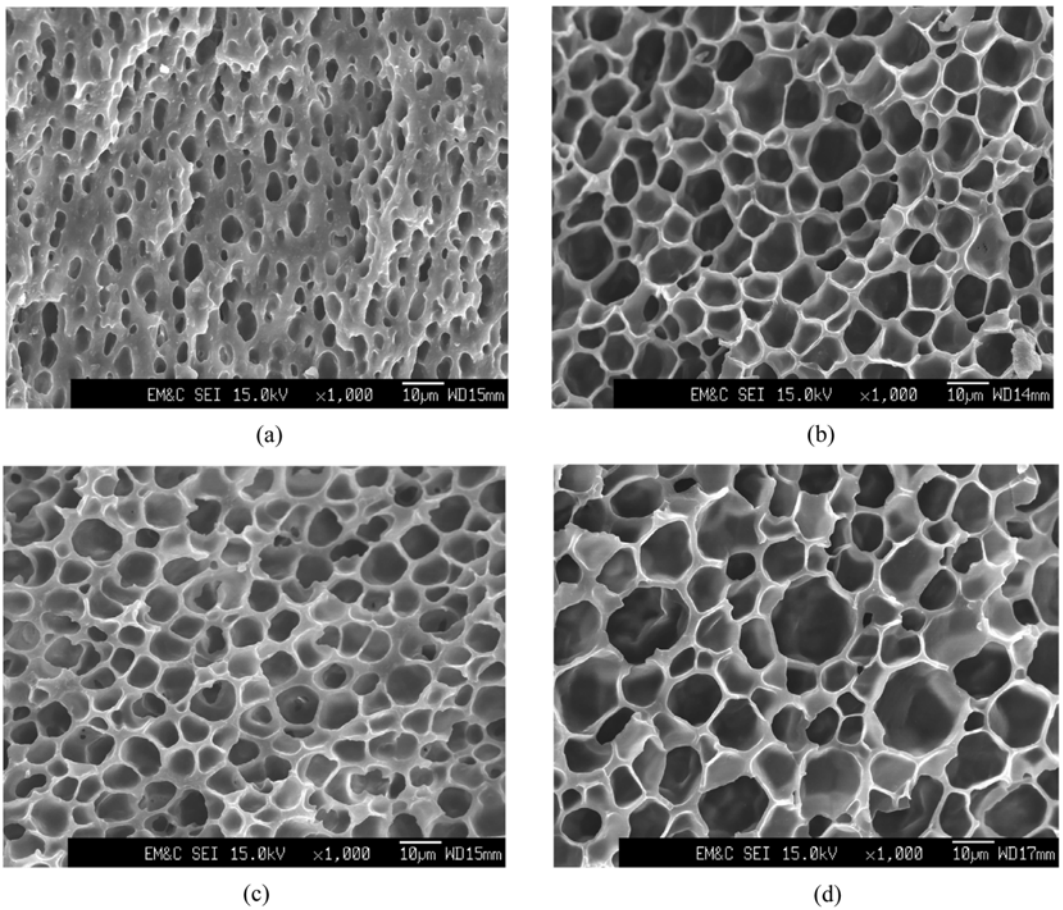

Fig. 6. SEM images of the freeze-fracture surface of EPDM/clay (100/5) nanocomposite foam processed at different temperatures: (a) 120 °C, (b) 125 °C, (b) 130 °C and (c) 135 °C.

Table 4. Morphological parameters of EPDM/clay (100/5) nanocomposite foam processed at different temperatures

	ρ_f (g/cm^3)	d (μm)	N_c (cell/cm^3)	δ (μm)
125 °C	0.22	7.74	1.64×10^{10}	1.14
130 °C	0.37	6.23	2.40×10^{10}	1.93
135 °C	0.25	10.6	5.94×10^{9}	2.00

EPDM/clay nanocomposite foam, therefore, should be attributed to much larger effective nucleation sites as compared to pure EPDM, which is provided by the fine dispersion of the clay particles in the nanocomposite. Effective increase in the modulus due to clay nanoparticles in the nanocomposite may restrain growth of cells and their coalescence, resulting in the reduction in the cell size of the foam as compared to the pure EPDM foam.

We also investigated effect of foam processing temperatures on the microstructure of EPDM/clay (100/5) nanocomposite foam. Fig. 6 shows the SEM image for the nanocomposite foams at different temperatures (120 °C, 125 °C, 130 °C, and 135 °C), and the morphological parameters of the foams are summarized in Table 4. It can be seen in Fig. 6(a) that when the foaming temperature is 120 °C, the sample was poorly foamed. Sufficient cell formation can be observed at elevated temperatures (Fig. 6(b), 6(c) and 6(d)) which are close to the melting temperature of the sample. It is noted that the foam processed at 135 °C has a larger cell size and decreased cell density as compared to that processed at 130 °C. This is probably because the material becomes weak with the increase in temperature and, thereby, above a critical temperature individual cells would coalesce into larger cells under high stretching force imposed onto the cell wall during the latter stages of cell growth.

CONCLUSIONS

Partially exfoliated nanocomposites could be fabricated by a melt blending of semicrystalline EPDM grafted with a small amount of maleic anhydride and an organoclay. A small amount of the clay nanolayers induce a remarkable increase in mechanical and dynamic mechanical properties of the rubber as well as an increase in non-isothermal crystallization rate. And, it was found that the nanocomposite can produce a closed-celled microcellular foam with average cell size as small as 6.2 μm and cell density as high as 2.4×10^{10} cell/cm^3 when the foaming was processed in supercritical CO_2.

ACKNOWLEDGEMENT

This work was supported by the SRC/ERC program of MEST (Grant R11-2005-056-04004-0).

REFERENCES

1. T. Lan and T. J. Pinnavaia, *Chem. Mater.*, **6**, 2216 (1994).
2. H. Shi, T. Lan and T. J. Pinnavaia, *Chem. Mater.*, **8**, 1584 (1996).
3. L. A. Utracki, *Clay-containing polymeric nanocomposites*, Rapra Technology Ltd., Shawbury, UK (2004).
4. J. W. Cho and D. R. Paul, *Polymer*, **42**, 1083 (2001).
5. T. D. Fornes, P. J. Yoon, H. Keskkula and D. R. Paul, *Polymer*, **42**, 9929 (2001).
6. S. R. Lee, H. M. Park, H. Lim, T. Kang, X. Li, W. J. Cho and C. S. Ha, *Polymer*, **43**, 2495 (2002).
7. Z. Liu, K. Chen and D. Yan, *Eur. Polym. J.*, **39**, 2359 (2003).
8. J. C. Huang, Z. Zhu, J. Yin, X. Qian and Y. Y. Sun, *Polymer*, **42**, 873 (2001).
9. N. Hasegawa, H. Okamoto, M. Kawasumi and A. Usuki, *J. Appl. Polym. Sci.*, **74**, 3359 (1999).
10. N. Hasegawa, H. Okamoto, M. Kato and A. Usuki, *J. Appl. Polym. Sci.*, **78**, 1918 (2000).
11. N. Hasegawa, H. Okamoto and A. Usuki, *J. Appl. Polym. Sci.*, **93**, 758 (2004).
12. K. H. Wang, M. H. Choi, C. M. Koo, Y. S. Choi and I. J. Chung, *Polymer*, **42**, 9819 (2001).
13. L. J. Lee, C. Zeng, X. Cao, X. Han, J. Shen and G. Xu, *Comp. Sci. Technol.*, **65**, 2344 (2005).
14. P. S. Chum, C. K. Kao and G. W. Knight, *Plast. Eng.*, **June**, 21 (1995).
15. P. H. Nam, P. Maiti, M. Okamoto, T. Kotaka, T. Nakayama, M. Takada, M. Ohshima, A. Usuki, N. Hasegawa and H. Okamoto, *Polym. Eng. Sci.*, **42**, 1907 (2002).
16. K. Taki, T. Yanagimoto, E. Funami, M. Okamoto and M. Ohshima, *Polym. Eng. Sci.*, **44**, 1004 (2004).
17. M. Mitsunaga, Y. Ito, S. S. Ray, M. Okamoto and K. Hironaka, *Macromol. Mater. Eng.*, **288**, 543 (2003).
18. Y. Ito, M. Yamashita and M. Okamoto, *Macromol. Mater. Eng.*, **291**, 773 (2006).
19. Y. Fujimoto, S. S. Ray, M. Okamoto, A. Ogami, K. Yamada and K. Ueda, *Macromol. Rapid Commun.*, **24**, 457 (2003).
20. Y. Di, S. Iannace, E. Di Maio and L. Nicolais, *J. Polym. Sci.: Part B: Polym. Phys.*, **43**, 689 (2005).
21. X. Han, C. Zeng, L. J. Lee, K. W. Koelling and D. L. Tomasko, *Polym. Eng. Sci.*, **43**, 1261 (2003).
22. W. Strauss and N. A. D'Souza, *J. Cell. Plast.*, **40**, 229 (2004).
23. C. Zeng, X. Han, L. J. Lee and K. W. Koelling, *Adv. Mater.*, **15**, 1743 (2003).
24. Y. W. Chang, D. S. Lee and S. Y. Bae, *Polym. Int.*, **55**, 184 (2006).
25. R. A. Vaia and E. P. Giannelis, *Macromolecules*, **30**, 8000 (1997).
26. L. Priya and J. P. Jog, *J. Polym. Sci. Part B: Polym. Phys.*, **41**, 31 (2003).
27. Z. Wang and T. J. Pinnavaia, *Chem. Mater.*, **10**, 3769 (1998).
28. R. Xu, E. Manias, A. J. Snyder and J. Runt, *J. Biomed. Mater. Res.*, **64A**, 114 (2003).
29. T. Amornsakchai, B. Sinpatanapan, S. Bualek-Limcharoen and W. Meesiri, *Polymer*, **40**, 2993 (1999).